General Disclaimer

One or more of the Following Statements may affect this Document

- This document has been reproduced from the best copy furnished by the organizational source. It is being released in the interest of making available as much information as possible.

- This document may contain data, which exceeds the sheet parameters. It was furnished in this condition by the organizational source and is the best copy available.

- This document may contain tone-on-tone or color graphs, charts and/or pictures, which have been reproduced in black and white.

- This document is paginated as submitted by the original source.

- Portions of this document are not fully legible due to the historical nature of some of the material. However, it is the best reproduction available from the original submission.

Produced by the NASA Center for Aerospace Information (CASI)

NATIONAL AERONAUTICS AND SPACE ADMINISTRATION

Technical Memorandum 33-489

Evaluation of Converters Fueled With Uranium Nitride

K. Shimada
P. L. Cassell

N71-32279

JET PROPULSION LABORATORY
CALIFORNIA INSTITUTE OF TECHNOLOGY
PASADENA, CALIFORNIA

July 30, 1971

Technical Memorandum 33-489

Evaluation of Converters Fueled With Uranium Nitride

K. Shimada

P. L. Cassell

PREFACE

The work described in this report was performed by the Guidance and
Control Division of the Jet Propulsion Laboratory.

CONTENTS

PRECEDING PAGE BLANK NOT FILMED

CONTENTS (Continued)

ABSTRACT

Two thermionic energy converters fueled with uranium nitride were fabricated and subjected to comprehensive tests to evaluate their performance as nuclear thermionic converters. Both converters had plane-parallel electrode geometry to increase the accuracy in making measurements of converter parameters and to simplify the laboratory testing which utilized an electron gun for the emitter heating. Of the two converters, one had a rhenium emitter and the other a tungsten emitter; the collector was niobium in both converters.

The evaluation of fuel-emitter compatibility, which was the major objective of the laboratory tests, was performed by measuring and correlating converter characteristics and electrode work functions.

The first phase of the evaluation, involving parametric testing, was completed. The initial performance of these converters was fully characterized so that any change that might occur during the second phase of the test, the life test, due to fuel-emitter interactions could be readily identified.

I. INTRODUCTION

Nuclear thermionic reactor power systems are potential candidates for supplying large amount of electric power for electric propulsion missions to the outer planets. Such reactors probably would be fueled with uranium oxide, uranium carbide, or uranium nitride (UN). Up to the present time there have been no investigations performed to determine the compatibility of UN, which is a high-performance nuclear fuel, with thermionic converters. At the Jet Propulsion Laboratory, a study was initiated under the Thermionic Reactor Systems Project to determine the effect of UN fuel on thermionic converter performance. The first phase of the evaluation involves the parametric tests and characterization of two UN-fueled converters, one having a rhenium emitter, the other a tungsten emitter. The second phase involves life tests to determine the long-term performance stability of the UN-fueled emitters.

The results of the parametric tests are described and presented in this report.

The maximum power density at 0.6 V, and at an emitter temperature of 2000°K, is 9.3 W/cm^2 for the UN-fueled rhenium converter and 3.8 W/cm^2 for the UN-fueled tungsten converter. The uncesiated work functions were 4.9 eV for the rhenium and 4.6 eV for the tungsten. The niobium collector work functions were 1.5 eV at a temperature ratio (collector temperature/cesium temperature) of 1.4 for both converters. The differences in converter power output are related with the difference in the measured work functions. Therefore, the in-situ work-function measurements of converters are quite valuable for evaluating the performance and correlating it with electrode changes resulting from nuclear fuel interactions during the life of the converter.

II. TEST APPARATUS

The converter was placed in a glass bell-jar, shown in Fig. 1, which was pumped by a 400 l/sec Vac-Ion pump. The background pressure in the bell-jar was kept in a 10^{-5}-N/m2 range with the converter at temperature. The pump system was equipped with a 15.24 cm high-vacuum gate valve and a titanium getter pump to minimize the time required for evacuating the bell-jar.

The emitter of the converter was electrically heated by an electron gun having a counter-wound tungsten filament which was placed approximately 0.3 cm away from the emitter. This filament was surrounded with two layers of tantalum sheet to reduce the glare entering into the optical pyrometer which was used for measuring the emitter temperatures.

The accelerating voltage of the electron gun was adjusted between 1 and 3 kV, depending on the emitter temperature, while the beam current was electronically maintained constant at any desired value so that the emitter temperature did not vary more than ±5°K from the preset value. The emitter temperature was measured at the blackbody hole by a Micro-Optical pyrometer; it was corrected for the bell-jar transmission and the pyrometer error by calibrating the measuring system against an NBS lamp.

The temperatures of the collector and the cesium reservoir were measured with chromel-alumel thermocouples which were connected to electronic reference junctions supplying 0°C reference voltages. The collector temperature was measured at 0.36 cm from the surface of the collector, and therefore the error in measured collector temperature was approximately 36°K when the heat flux was 100 watts. The cesium reservoir temperature was measured with a negligible error at a liquid-vapor interface. Both the collector and the reservoir temperatures were maintained within ±1.0°K of the preset values by means of two proportional temperature controllers shown in the console (Fig. 1). On this console, there are (from the top): (1) two digital monitors,

(2) two temperature programmers, (3) two heater supplies, (4) a 6-place digital voltmeter for temperature measurements, (5) two proportional controllers, (6) a 25-channel input scanner, and (7) a multi-channel temperature monitor. The console on the right contains high-voltage supplies for the electron gun.

The volt-ampere curves were obtained using an X-Y recorder mounted on a smaller console (data console) which also contained an electronic power supply for the converter under test. This power supply (Ref. 1) is capable of operating in either a steady-state or a pulsed mode, depending upon the static or dynamic mode of data acquisition. In the steady-state mode, the output voltage of the power supply is manually adjusted so that a static volt-ampere curve can be acquired. In the pulsed mode, the output voltage is modulated by a train of square pulses having a repetition rate of 25 pulses per second. Each pulse has a fast rise time compared with its duration of 300 μsec; the pulse height varies monotonically between a maximum and a minimum passing through zero where the output voltage corresponds to the static operating point. When the pulse is on, the converter current attains a quasi-static value toward the end of each pulse, at which time the voltage across and the current through the converter are electronically sampled for 40 μsec, stored, and displayed as one data point on the X-Y recorder. This process repeats at a rate of 25 points/second. On the average, there are 250 of such data points on one dynamic volt-ampere curve when the converter voltage is swept in 10 seconds. Since this dynamic data acquisition requires a small duty cycle (0.75%), a volt-ampere characteristic is isothermally obtained at temperatures of a converter which are preset at the static operating point of the converter. Also, these temperatures can cover a wide range because the data acquisition does not influence the temperatures as it would in an ordinally dynamic method utilizing a 60-Hz sweep. Therefore, the pulsed data acquisition is flexible, accurate, and fast in obtaining desired volt-ampere curves.

III. UN-FUELED RHENIUM CONVERTER CONSTRUCTION

The construction of the converter, shown in Fig. 2, is similar to that described by T. Speidel (Ref. 2); however, the JPL converter is fueled with uranium nitride. The electrode geometry is plane-parallel; the emitter area is 1.82 cm^2, and the interelectrode space is 0.025 cm. The emitter material is arc-cast rhenium, and the collector material is niobium. The nitride fuels are placed in 7 cylindrical holes in the body of the emitter with the fuel volume fraction equalling 0.259.

The distance between the bottom of the holes and the emitter surface is 0.0635 cm (Fig. 3), and the opposite side of the emitter is capped with a rhenium disk 0.0635-cm thick. A blackbody hole, having a diameter-to-depth ratio of 7.33 is drilled parallel to the emitter surface with its axis at 0.302 cm from the surface. The collector calorimeter, which is mechanically fastened to a water-cooled heat sink, and the collector itself are machined from one piece of niobium.

To evaluate the performance of this converter, the parametric tests were made during the initial test period. These tests consisted of the measurement of static and dynamic volt-ampere curves. The electrode work functions were also determined from the dynamic volt-ampere curves that were obtained with the pulsed data system described in Section II. The work functions will be used to evaluate the fuel-electrode interactions that might occur during the subsequent life test.

A. Emitter Work Function

To determine the nuclear fuel effects (if any) on the thermionic emitter, the emitter work function ϕ_E was carefully determined from temperature saturated currents of the converter obtained from dynamic volt-ampere curves. The emitter work functions were calculated from the Richardson equation by using the measured saturation current I_S and the emitter temperature T_E as shown below:

$$I_S/1.82 = 120\ T_E^2 \exp(-\phi_E/kT_E) \qquad (1)$$

where 1.82 is the emitter area in cm^2 and k is the Boltzmann constant (1.38×10^{-23} J/°K $= 0.863 \times 10^{-4}$ eV/°K). The emitter temperature T_E was determined from the true blackbody temperature T_B because there is no temperature correction required during the work-function measurements which are performed under small heat-flux conditions. During these measurements, the cesium reservoir temperature T_R was kept at those values which allowed the converter to operate in an ion-rich, unignited mode with a negligible amount of electron scattering. Therefore, the measured saturated current I_S was temperature saturated so that Eq. (1) is valid. Typical volt-ampere curves showing temperature-saturated currents are shown in Fig. 4. The saturation current was determined from the intersection of two straight lines that approximated the saturation and Boltzmann part of the volt-ampere curve. Any one particular volt-ampere curve was obtained with constant emitter temperature (±5.0°K) constant cesium temperature (±0.5°K) and constant collector temperature (±1.0°K). The work functions calculated from Eq. (1) are shown in Fig. 5 as a function of the temperature ratio T_E/T_R. It should be pointed out that the cesium temperature T_R was corrected for the cesium transpiration effect that exists at low temperatures where the atomic mean free path is considerably larger than the interelectrode gap. Temperature corrections of approximately 10°K were required for T_R in these cases. The results given in Fig. 5 show that the cesiated work function of this emitter agreed with that of a material having an uncesiated work function ϕ_O of 4.9 eV. The value for this arc-cast rhenium emitter is in good agreement with that for polycrystalline rhenium.

B. Collector Work Function

The work function ϕ_C of the niobium collector was spot-checked by a method using volt-ampere curves, such as shown in Fig. 6, in an electron-retarding voltage region. These two volt-ampere curves shown in a semi-log plot correspond to two different collector temperatures. During the measurements, temperatures of the emitter and the collector were limited to those which did not cause appreciable ion currents nor back emission currents. Also the reservoir temperatures were kept at relatively small values so that the converter current would show both a saturation and a Boltzmann region, and the converter would operate in an unignited mode. Under these conditions, the current I is related to the converter voltage by the following equation:

$$I = I_S \exp(\phi_E - \phi_C - eV)/kT_E \qquad (2)$$

for

$$eV \geq eV_R = \phi_E - \phi_C \qquad (3)$$

where V_R is the voltage at which two straight lines, approximating the saturation and the Boltzmann current, intersect (Fig. 6) and

$$I = I_S \text{ for } eV \leq eV_R. \qquad (4)$$

Therefore, the collector work function ϕ_C can be determined from an equation

$$\phi_C = \phi_E - eV_P \qquad (5)$$

where

$$I = I_S$$

The work function ϕ_E used in Eq. (5) was determined from the Richardson equation:

$$I_S/1.82 = 120\ T_E^2 \exp(-\phi_E/kT_E). \qquad (6)$$

The values of ϕ_C were 1.53 at T_C/T_R of 1.44, and 1.54 at T_C/T_R 1.42. These results are approximately 0.2 eV lower than work functions expected for a cesiated niobium collector.

C. Static Volt-Ampere Curve

To evaluate the power-output performance of the converter, three static volt-ampere curves such as those shown in Fig. 7 were obtained at true blackbody emitter temperatures T_B, of 1800, 1900 and 2000°K. The static data points were taken at output voltages of 0.4, 0.6, 0.8, and 1.0V. The output current was maximized for each voltage by adjusting T_R and T_C. The temperature ratio T_B/T_R, required to maximize the output current and, hence, the output power at that voltage, increased almost linearly with the output voltage as shown in Fig. 8; for example, $T_B/T_R = 3.24$ and 3.42 at 0.4 and 1.0 volts output, respectively, for a case with $T_B = 2000$°K. In contrast, T_C/T_R was practically independent of the converter output and the emitter temperature. The results indicated that, at an increased output voltage at which the output current was small the optimum T_B/T_R as well as ϕ_E were large, whereas the optimum T_C/T_R remained fairly constant at $T_C/T_R \simeq 1.4$, at which the collector work function ϕ_C was slightly larger than its minimum value. It appeared that if the T_C/T_R were

such that ϕ_C was a minimum, the collector back emission adversely affects the power output. A large amount of back emission results in a negative space-charge sheath at the collector, which in turn increases the collector surface barrier.

Maximum power densities are plotted in Fig. 9 as a function of output voltage V. The results show that the maximum power density was 8.8 W/cm^2 at V ~ 0.61 for T_B ≈ 2000°K, and that it was 6.7 W/cm^2 at V ~ 0.47 for T_B ≈ 1800°K. These power densities are comparable with those in other rhenium converters having an interelectrode gap of 0.254 mm (Ref. 3). The output voltages at which the maximum power densities occur for a given emitter temperature are shown to lie on a straight line passing through the origin. The current densities at maximum power point remained unchanged at 14.5 A/cm^2 for all temperatures.

D. Emitter Surface Temperature

To obtain further insight into converter performance and to relate its performance with emitter surface properties, the emitter temperature T_E was calculated from the blackbody temperature T_B by using the following equation:

$$T_E = T_B - R_T Q \qquad (7)$$

where R_T is the inverse of the thermal conductance of the emitter and Q is the heat flux. Since there were 7 holes in this button to hold the UN-fuel pellets, the total thermal conductance was determined to be the sum of thermal conductances for the fuel and the metal portions (rhenium) of the emitter. Assuming that the fuel completely filled each hole, one obtains

$$1/R_T = 1/R_H + 1/R_{Re} \qquad (8)$$

where $1/R_H$ and $1/R_{Re}$ are the thermal conductances of the hole and the rhenium portion of the emitter. By using thermal conductivity values (Ref. 3) of 0.313 W/cm - °C for UN-fuel pellets and 0.680 W/cm - °C for rhenium metal, the equivalent thermal resistance R_T, between the surface and the blackbody hole, was calculated to be 0.386°C/W. Therefore, Eq. (7) can be rewritten as follows:

$$T_E = T_B - 0.386 \ Q. \qquad (9)$$

Since the heat flux Q is the sum of thermal radiation from the emitter to the collector, the cesium gas conduction, the electron cooling, and other stray heat flux (which was assumed to be 20 percent of the sum), Q is therefore a function of the surface temperature and the converter current. Furthermore, the cesium conduction, which is a relatively small term, is practically constant in the range of temperatures in which the converter was operated. Therefore, a set of curves (Fig. 10) that relate T_B with T_E are obtained for various converter currents. For example, at T_B = 2000°K, I_O = 26.5 A (14.5 A/cm^2), and V = 0.6 V, the surface temperature T_E is

1944°K; the total heat flux in this case is 144 W, which consists of 30.9, 3.7, and 85.4 and 24.0 watts of radiation, cesium conduction, electron cooling, and stray heat flux respectively. Therefore, at this point, the converter efficiency was 11 percent. At other static operating points, shown in Fig. 7, the surface temperature was lower than the blackbody temperature by a maximum of 67°K and a minimum of 25°K. In Section 5, the converter output is expressed as a function of the converter voltage for different surface temperatures T_E that were obtained from temperature calibration curves, as shown in Fig. 10.

E. Dynamic Volt-Ampere Curves

To evaluate further the characteristics of the power-producing converter, dynamic volt-ampere curves were obtained under constant temperature conditions by using the method described in Section II. Results obtained with the blackbody temperatures at 1800, 1900, and 2000°K are shown in Figs. 11, 12, and 13. A group of curves in each figure represent volt-ampere characteristics where only the cesium reservoir temperature was varied. For example, in Fig. 12, a volt-ampere curve for a case with T_B = 1900°K and T_R = 595°K, was obtained by: (1) setting the static operating point at 0.45 V, (2) letting the converter stabilize at pre-selected temperatures, (3) superimposing a train of voltage pulses on the static voltage (0.45 V) to dynamically sweep the converter voltage, and (4) recording the sampled voltage across and the current through the converter by an X-Y recorder at the rate of 25 points per second. During each sweep of the volt-ampere curve, all temperatures remained unchanged since the duty cycle of the pulse train was 0.75 percent.

An envelope of curves showing the upper limit of the converter performance at T_B = 1900°K and T_C = 840°K is also shown in Fig. 12. A volt-ampere curve that is tangent to this envelope at a certain output voltage has a unique cesium reservoir temperature which coincides with the optimum reservoir temperature for a given T_B and T_C. For example, at V = 0.6 V, a volt-ampere curve with T_R = 590°K is tangent to an envelope for T_B = 1900°K, T_C = 840°K. According to the static volt-ampere curve shown in Fig. 7 for T_B = 1900°K and T_C = 806°K, the optimum T_R was also 590°K as was expected. This fact clearly shows that an envelope of dynamic volt-ampere curves, which are obtained under isothermal conditions by using the pulsed-mode apparatus, can replace static volt-ampere curves, which require a considerable length of time for optimization and stabilization; in fact, the three envelopes for T_B = 2000, 1900, and 1800°K, shown in Fig. 14, are practically identical to the static volt-ampere curves shown in Fig. 7 for the same emitter temperatures. The results demonstrate the expediency, accuracy and flexibility of the pulsed dynamic data acquisition.

After applying the temperature corrections shown in Eq. (9), the curves shown in Fig. 14 were redrawn (Fig. 15) to correlate the output performance with the surface temperature T_E. The results show that the power density was as large as 9.3 W/cm^2 at 15.5 A/cm^2 and 0.6 V

when the emitter surface temperature T_E was 2000 K. The performance was slightly better than expected as the result of: (1) a slightly larger bare emitter work function (ϕ_0 = 4.9 eV), and (2) a small cesiated collector work function (ϕ_C = 1.5 eV). The nuclear fuel in the emitter should not have influenced the performance during these measurements. Any variation in the performance during subsequent life tests can be accurately correlated with the initial results.

V. UN-FUELED TUNGSTEN CONVERTER

Another converter, identical in construction to the rhenium converter except for having a tungsten emitter and just one hole with a UN-fuel pellet (Fig. 2), was also parametrically tested. Three families of volt-ampere curves, shown in Figs. 16, 17, and 18, were acquired at T_B = 2000, 1900, and 1800°K by the pulsed dynamic method. The envelopes of these curves were constructed and plotted as shown in Fig. 19. Comparisons made between the two converters, shown in Fig. 20, indicated that the output current of the tungsten converter was less than one half of that of the rhenium converter operating at the same emitter temperature and voltage. The emitter work function shown in Fig. 21 indicated that the bare work function of the tungsten emitter is 4.6 eV, which is in agreement with that of a polycrystalline tungsten; the collector work function was 1.55 eV at T_C/T_R = 1.5, as was expected from similar measurements on the rhenium converter. In view of these findings, the inferior performance of the tungsten converter was attributed partially to the low bare work function (4.6 eV) of its emitter, unlike that in the rhenium converter.

The emitter surface temperature T_E of this converter can be calculated from,

$$T_E - T_B - 0.163\ Q.\qquad(10)$$

According to this equation, the correction in temperature, 0.163 Q, was approximately 10°K at T_B = 2000°K, output voltage = 0.6 V and output current = 6.1 A/cm². The correction, which was much smaller than that for the rhenium converter, resulted from: (1) larger thermal conductivity of tungsten, and (2) smaller electron cooling flux because of the smaller output current of the tungsten converter. Thus, the output power density of this converter which was 3.7 W/cm² at T_B = 2000°K is equivalent to 3.7 W/cm² at T_E = 1990°K. The power density also can be extrapolated to 3.8 W/cm² at T_E = 2000°K. Therefore, the performance of this converter which was expressed in terms of the blackbody temperature T_B can be considered identical, within an experimental error, to that with the surface temperature T_E.

VI. CONCLUSIONS

A comprehensive investigation is underway to evaluate the effect of uranium nitride as a nuclear fuel on thermionic converter performance. The first phase of this investigation, to build and characterize two UN-fueled converters for initial performances, is completed. Of the two converters studied, the rhenium-emitter converter produced an output power density of 9.3 W/cm^2 at 0.6 V with T_E = 2000°K which was equivalent to 8.8 W/cm^2 with T_B = 2000°K. The tungsten-emitter converter produced a power of 3.8 W/cm^2 with T_E = 2000°K or 3.7 W/cm^2 with T_B = 2000°K which was less than one half of the rhenium-emitter converter. The difference in performance is partially accounted for by the difference in the emitter work functions which are 4.9 eV for rhenium and 4.6 eV for the tungsten. The collector work function is approximately 1.5 eV for both converters.

The data acquisition system, utilizing a small duty-cycle, pulsed power supply in conjunction with a sampled-data system, proved to be versatile, accurate and fast in acquiring static as well as dynamic volt-ampere characteristics. Accurate in-situ measurements of electrode work functions provides an additional parameter that is useful in predicting converter performance and evaluating its change.

In the second phase of the program, these two converters will be life-tested. The long range effects of UN-fuel on the converter performance will be examined by comparing converter power output and work functions during life tests with the initial power output and work functions determined in this first phase.

REFERENCES

1. K. Shimada and P. L. Cassell, "Small-Duty-Cycle Data Acquisition in Thermionic Research", JPL SPS 37-49, Vol. III, pp. 130-132, December 1967/January 1968.

2. T. O. Speidel and R. M. Williams, "Fixed-Space Planar Thermionic Diode with Collector Guard Ring," IEEE Record of Thermionic Conversion Specialist Conference, pp. 113-117, October 1968.

3. O. S. Merrill "Correlation of Fixed-Spacing Thermionic Converter Performance with Variable-Spacing Test Vehicle Data," IEEE Record of Thermionic Conversion Specialist Conference, pp. 103-112, October 1968.

4. Private Communication with F. Rufeh, Thermo Electron Co., Waltham, Mass.
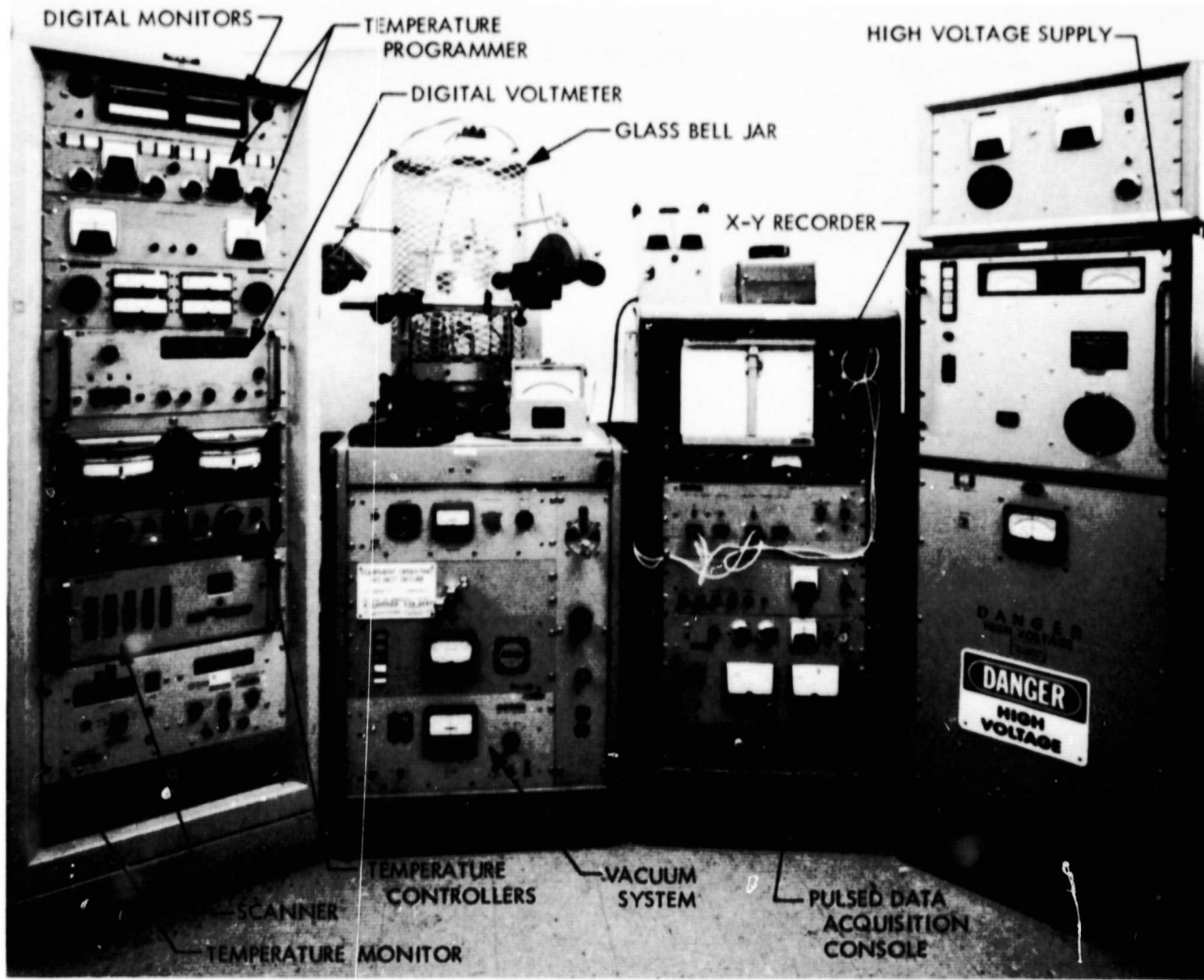
Fig. 1. Photograph of the test Setup
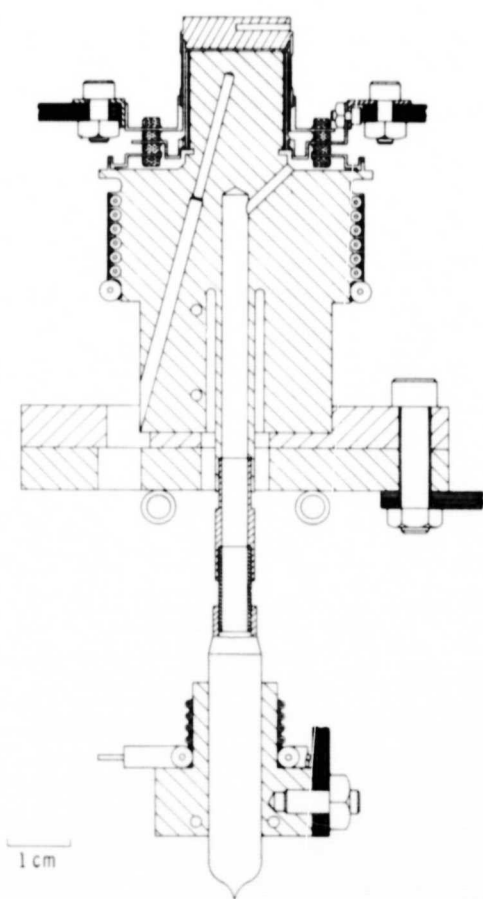
Fig. 2. Schematic Drawing of the Converter
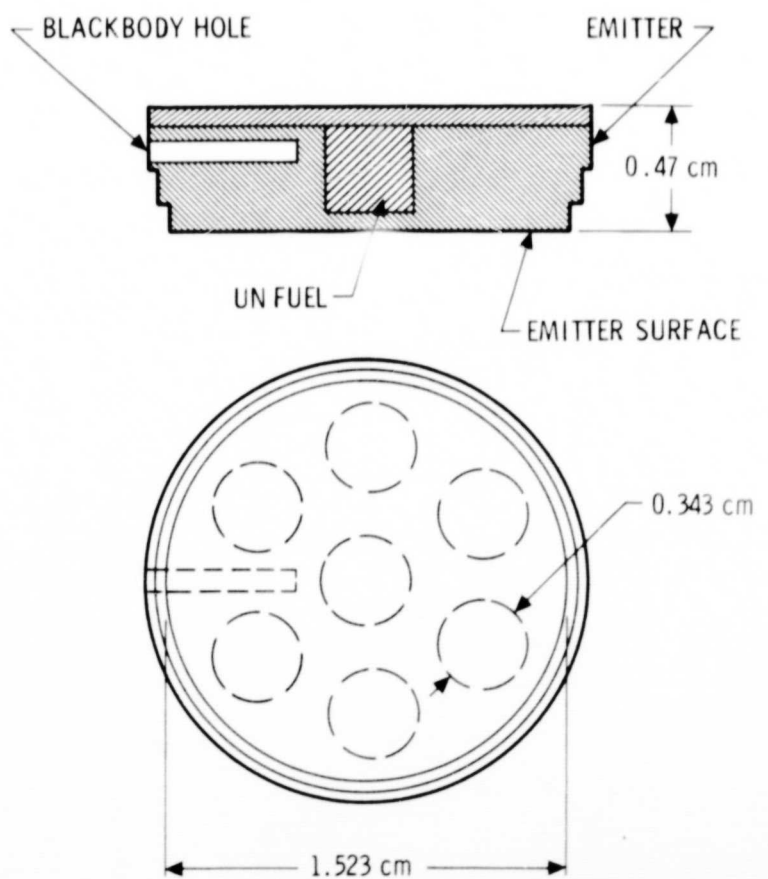
Fig. 3. Fueled Emitter Detail
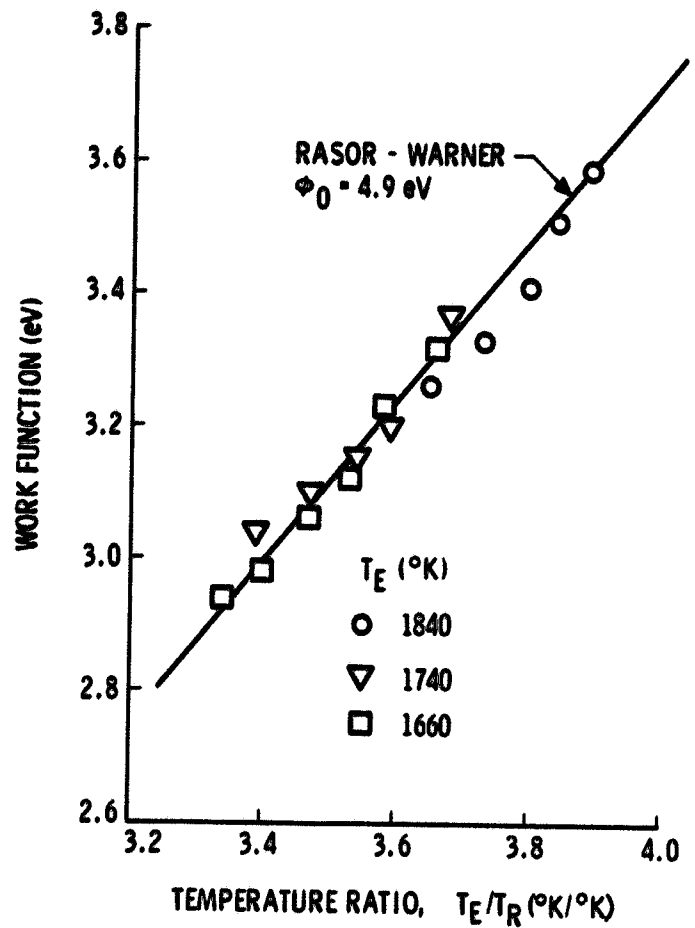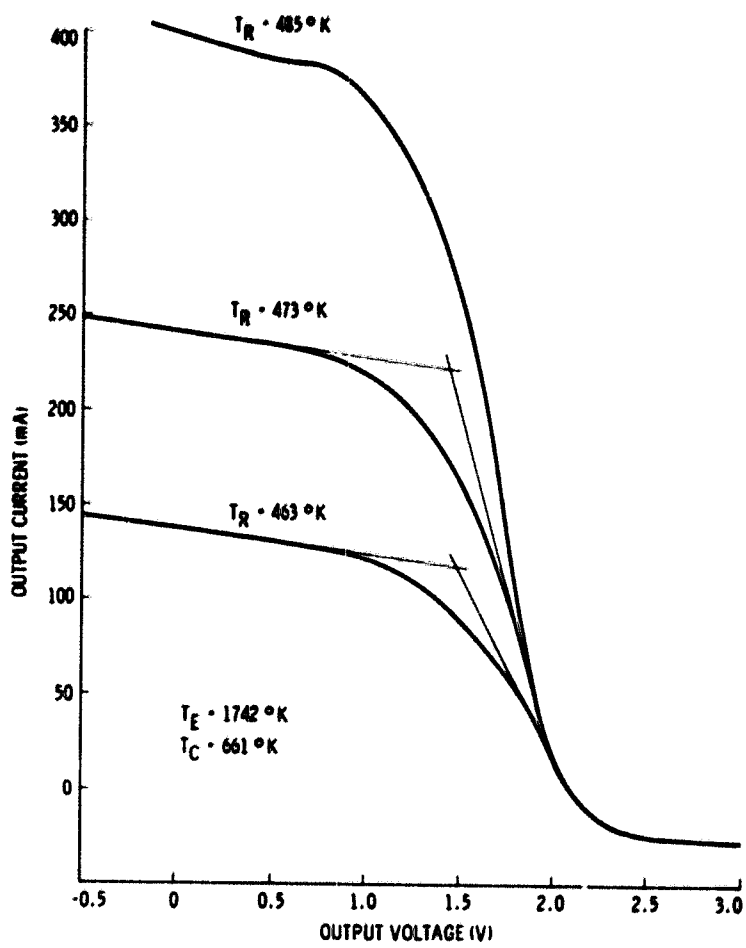
Fig. 4. Volt-Ampere Curves for Emitter
Work Function Measurements

Fig. 5. Rhenium Emitter Work Function
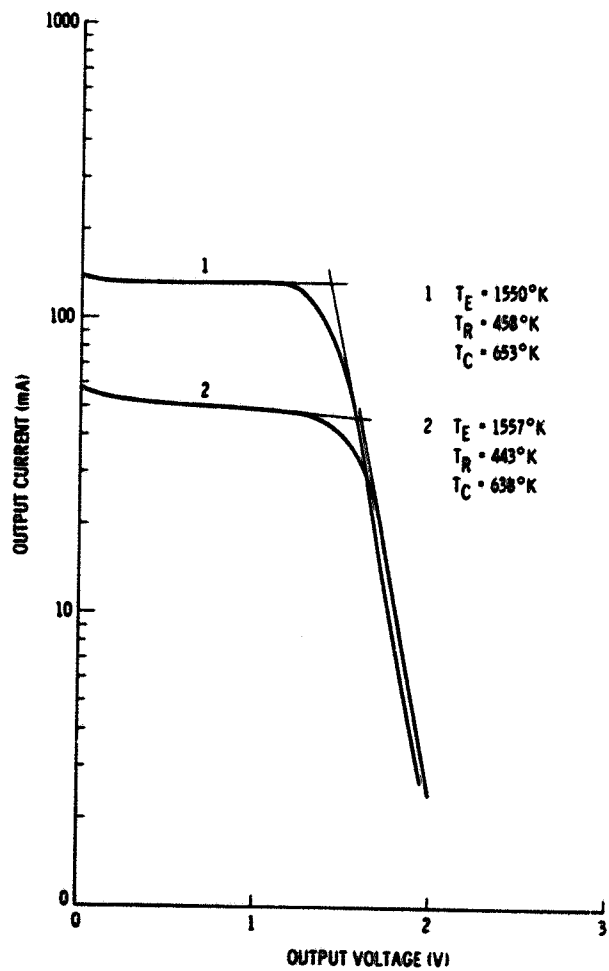
Fig. 6. Volt-Ampere Curves for Collector
Work Function Measurements
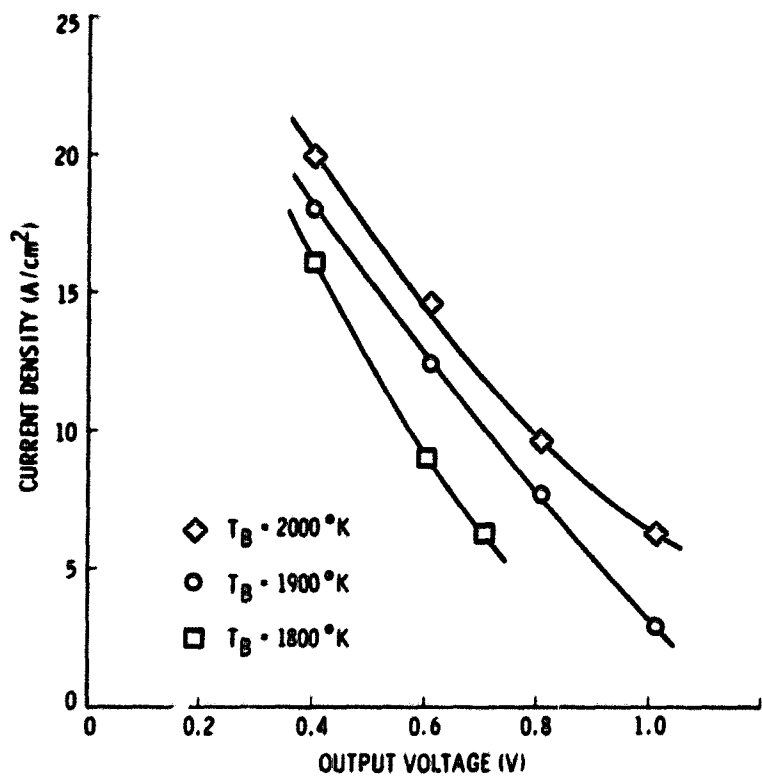
Fig. 7. Static Volt-Ampere Curves at T_B = 1800, 1900 and 2000°K, Rhenium Converter

Fig. 9. Power Density versus Output Voltage, Rhenium Converter

Fig. 8. Optimum Temperature Ratios, Rhenium Converter
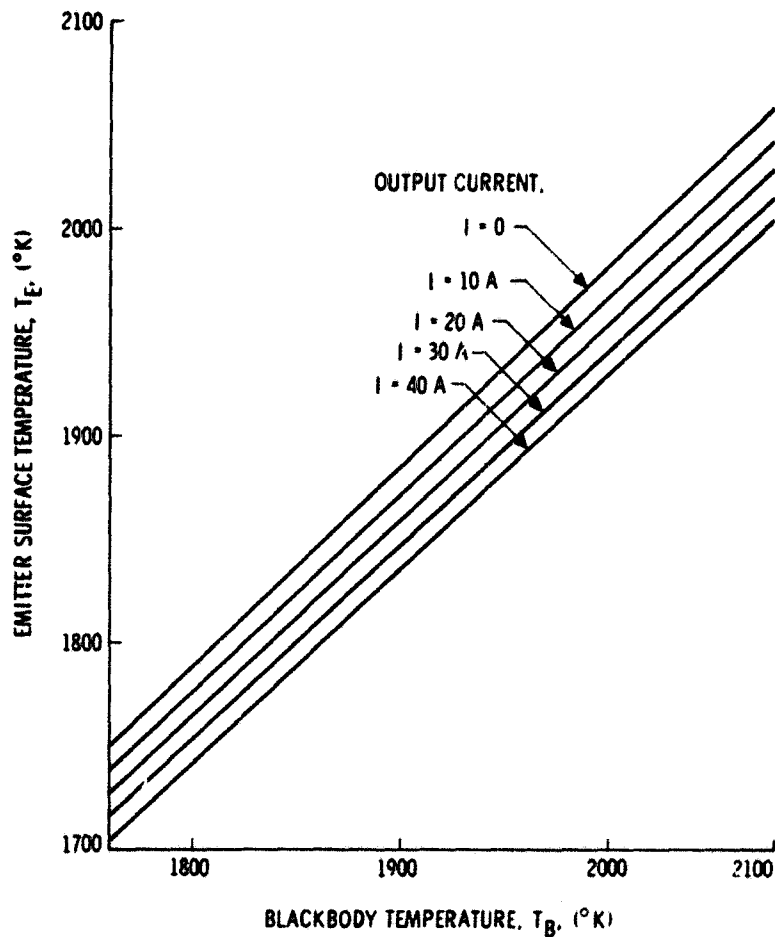
Fig. 10. Temperature Correction Curves, Rhenium Converter
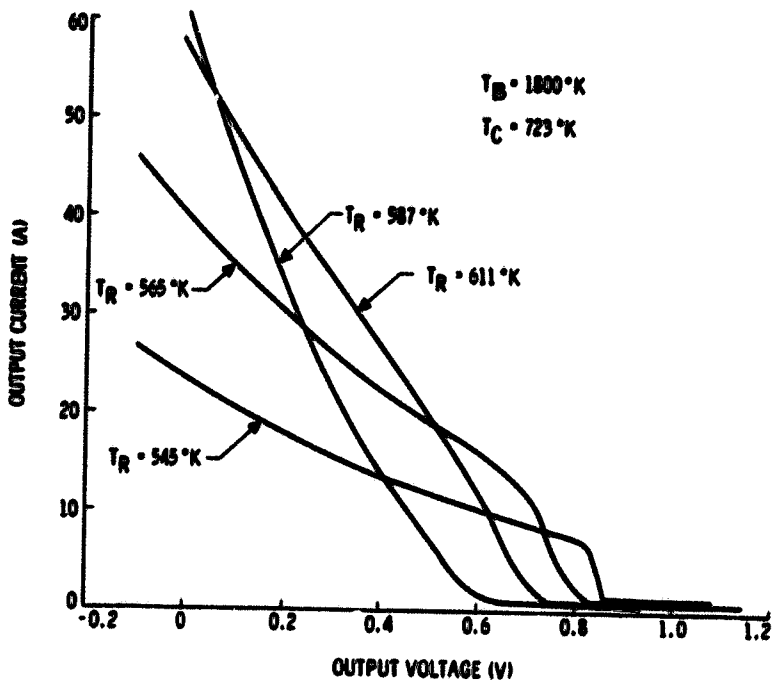
Fig. 11. Dynamic Volt-Ampere Curves,
Rhenium Converter, $T_B = 1800°K$
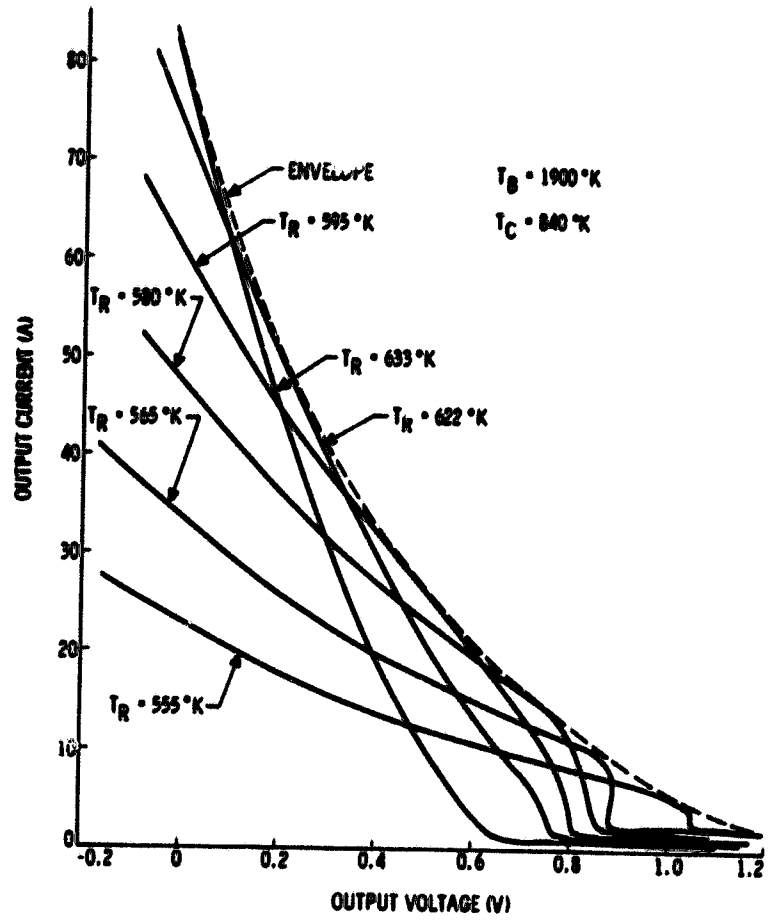
Fig. 12. Dynamic Volt-Ampere Curves,
Rhenium Converter, $T_B = 1900°K$
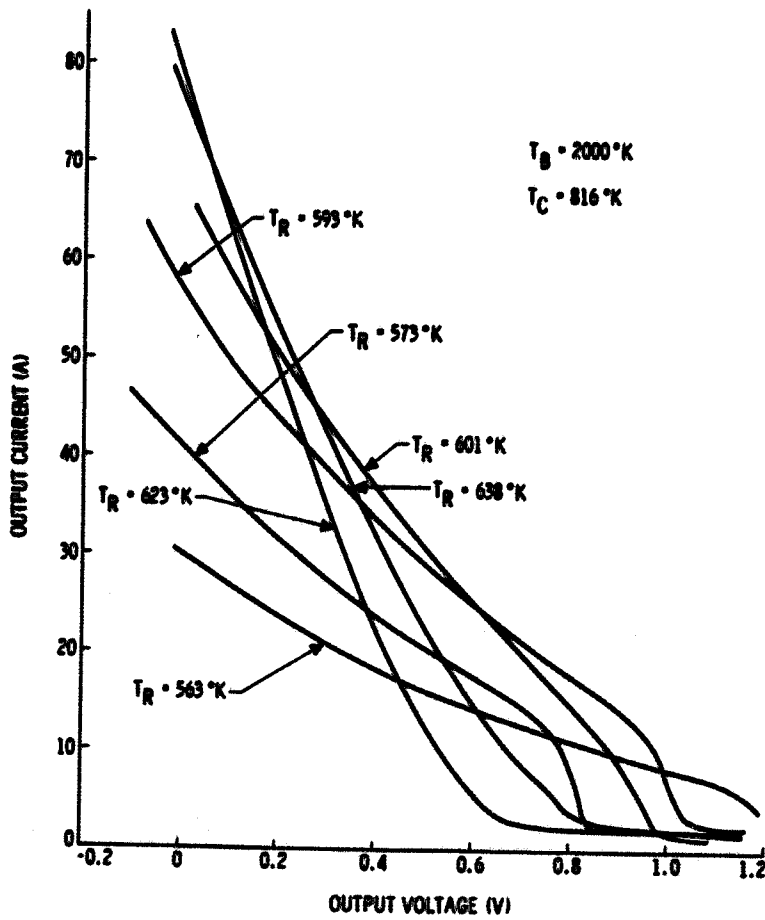
Fig. 13. Dynamic Volt-Ampere Curves,
Rhenium Converter, $T_B = 2000°K$
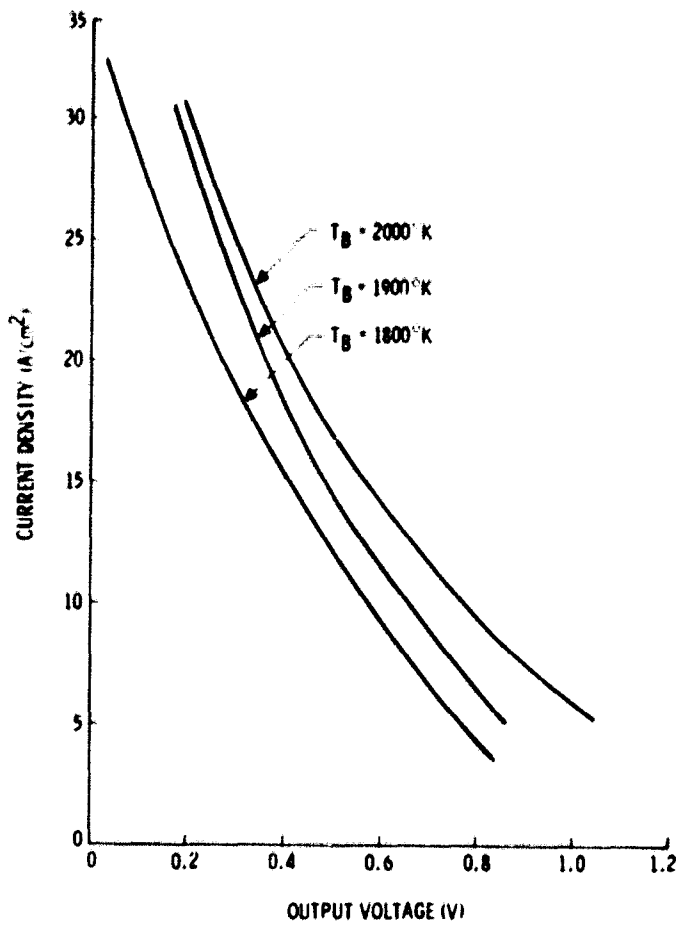
Fig. 14. Envelopes of Dynamic V-A Curves for Rhenium Converter, T_B = 1800, 1900 and 2000°K
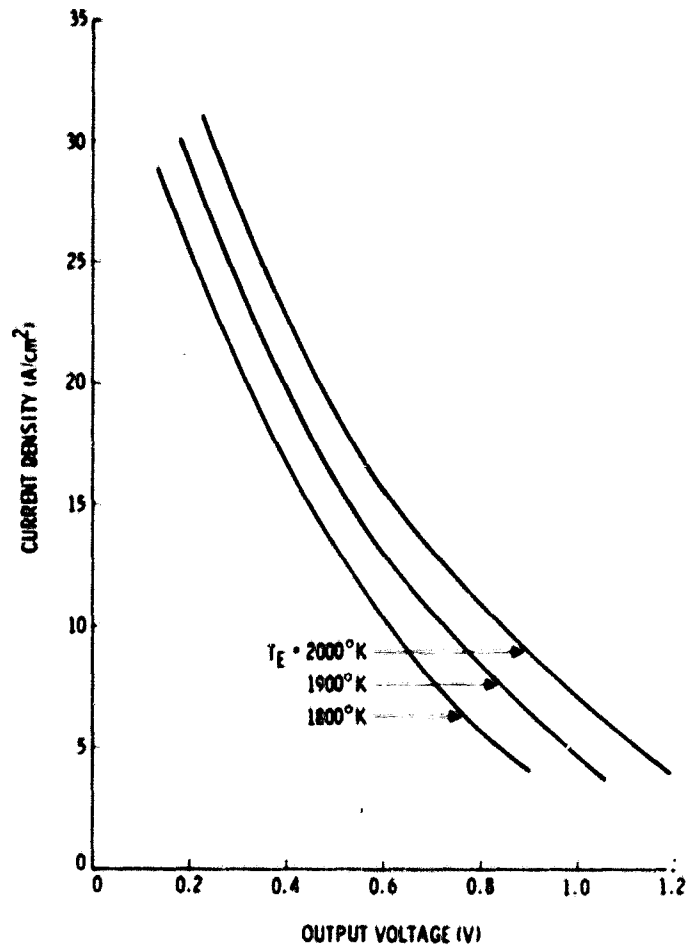
Fig. 15. Envelopes of Dynamic V-A Curves, for Rhenium Converter, T_E = 1800, 1900 and 2000°K
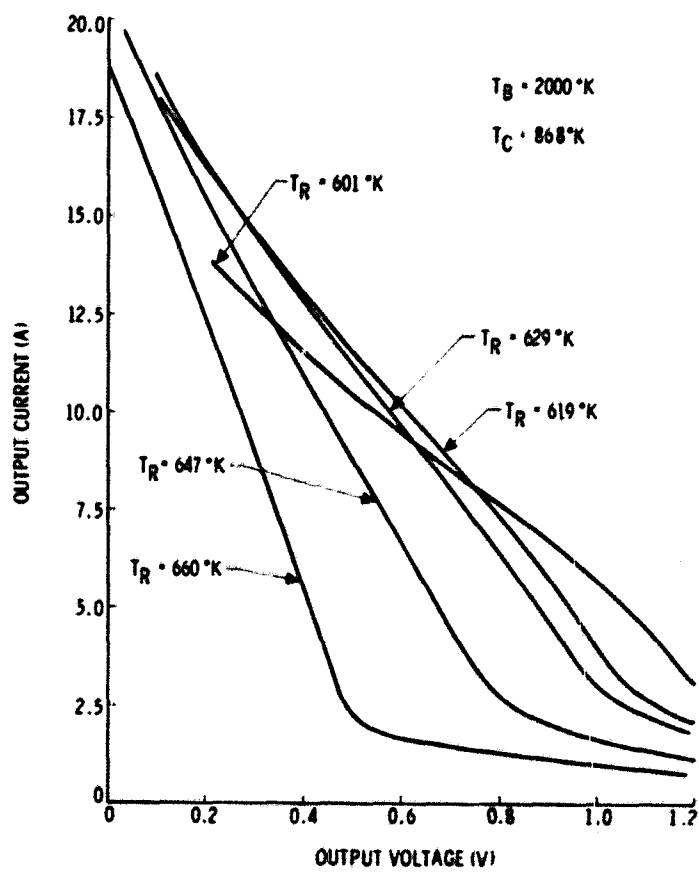
Fig. 16. Dynamic Volt-Ampere Curves, Tungsten Converter, T_B = 2000°K
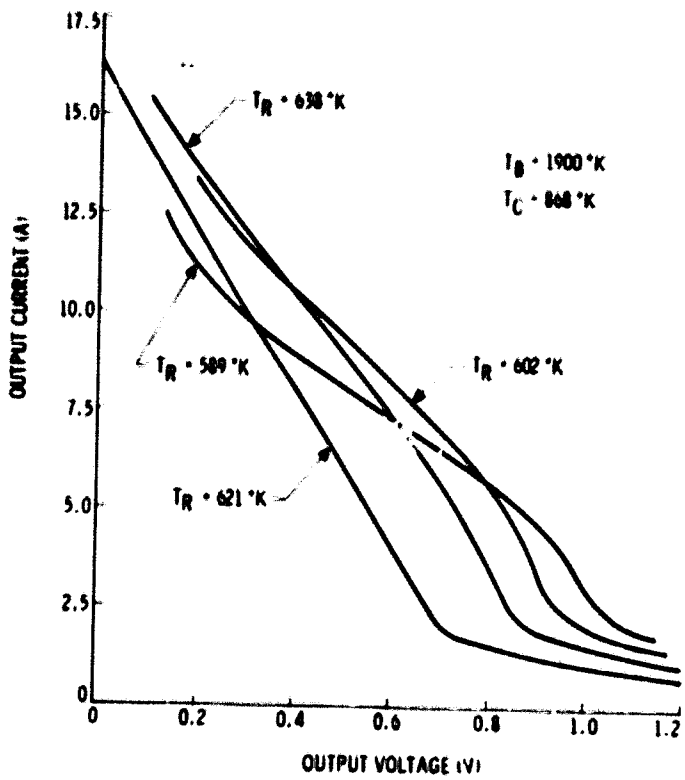
Fig. 17. Dynamic Volt-Ampere Curves,
Tungsten Converter, T_B = 1900°K
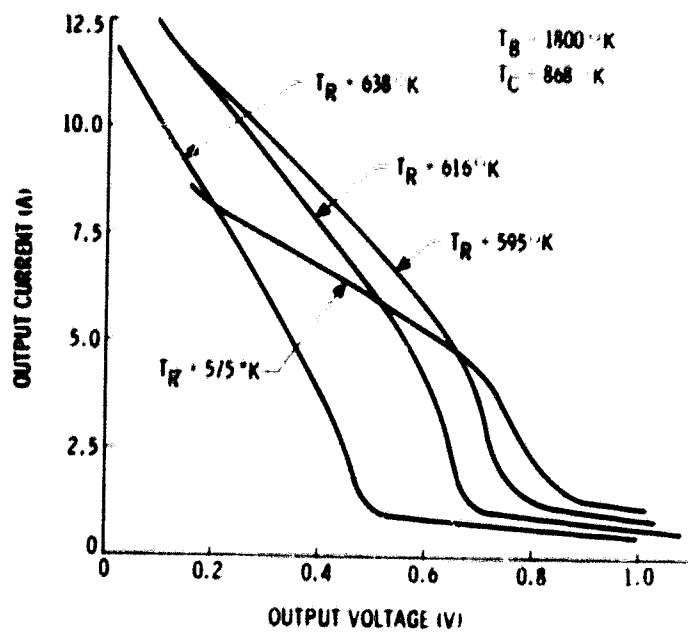
Fig. 18. Dynamic Volt-Ampere Curves,
Tungsten Converter, T_B = 1800°K
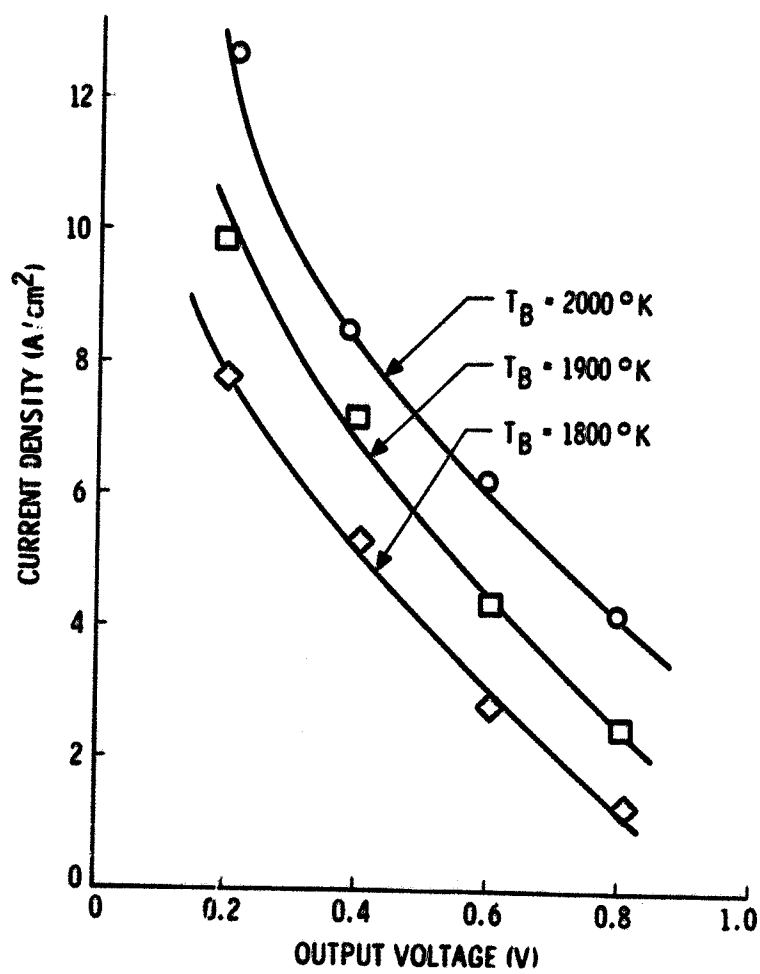
Fig. 19. Envelopes of Dynamic V-A Curves
for Tungsten Converter

14
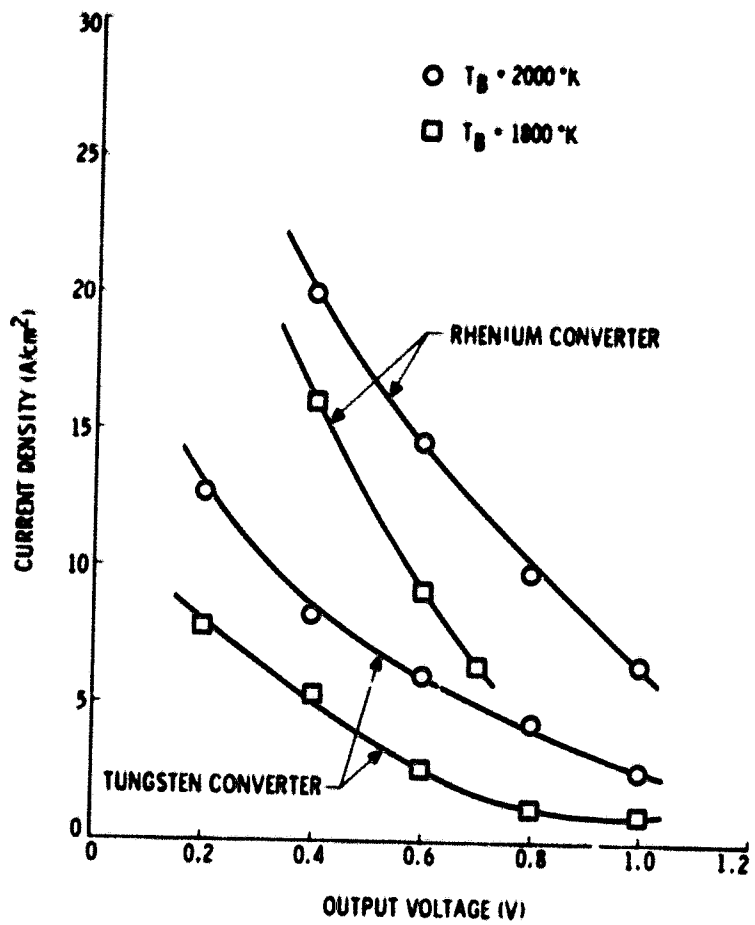
Fig. 20. Performance Comparison
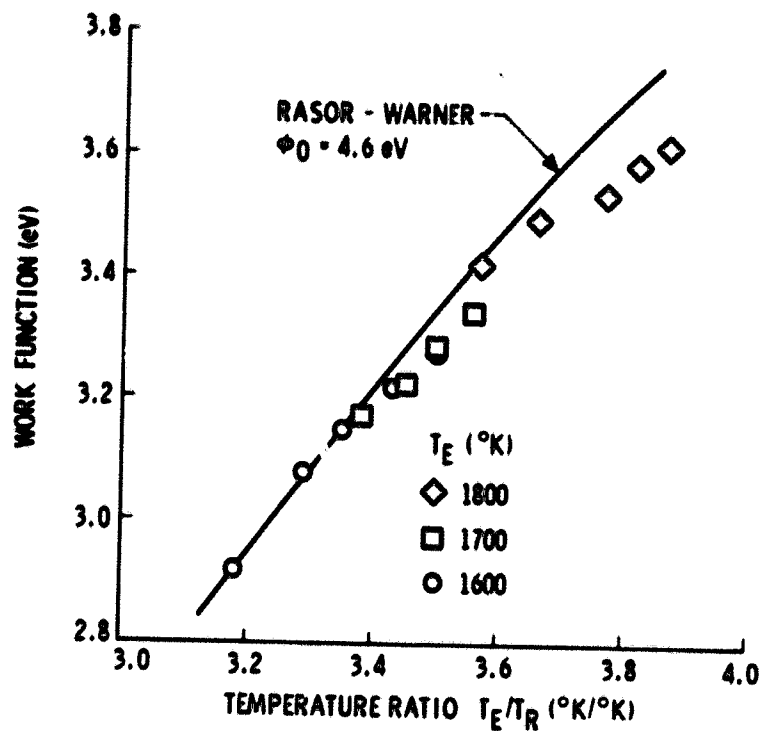
Fig. 21. Tungsten Emitter Work Function